Atmospheric Environment 182 (2018) 225–233

Contents lists available at ScienceDirect

Atmospheric Environment

journal homepage: www.elsevier.com/locate/atmosenv

Temporal and spatial characteristics of dust devils and their contribution to the aerosol budget in East Asia—An analysis using a new parameterization scheme for dust devils

Yaoguo Tang[a], Yongxiang Han[a,b,*], Zhaohuan Liu[a]

[a] Collaborative Innovation Center on Forecast and Evaluation of Meteorological Disasters, Nanjing University of Information Science and Technology, Nanjing, 210044, China

[b] Key Laboratory for Aerosol-Cloud-Precipitation of China Meteorological Administration, Nanjing University of Information Science & Technology, Nanjing, 210044, China

GRAPHICAL ABSTRACT

A new parameterization scheme for dust devils was established and coupled with WRF-Chem, the diurnal and monthly spatial distribution and intensity of dust devils in northern China were given for the first time. Simulated monthly distribution and intensity of dust devils in 2009 (a: April; b: May; c: June; d: July; e: August; f: September).

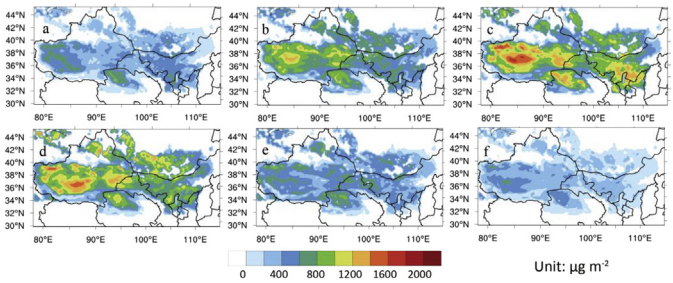

ARTICLE INFO

Keywords:
Contribution rate
Diurnal variation
Monthly variation
Dust devil
Atmospheric dust aerosols

ABSTRACT

Dust aerosols are the main aerosol components of the atmosphere that affect climate change, but the contribution of dust devils to the atmospheric dust aerosol budget is uncertain. In this study, a new parameterization scheme for dust devils was established and coupled with WRF-Chem, and the diurnal and monthly variations and the contribution of dust devils to the atmospheric dust aerosol budget in East Asia was simulated. The results show that 1) both the diurnal and monthly variations in dust devil emissions in East Asia had unimodal distributions, with peaks in the afternoon and the summer that were similar to the observations; 2) the simulated dust devils occurred frequently in deserts, including the Gobi. The distributed area and the intensity center of the dust devil moved from east to west during the day; 3) the ratio between the availability of convective buoyancy relative to the frictional dissipation was the main factor that limited the presence of dust devils. The position of the dust devil formation, the surface temperature, and the boundary layer height determined the dust devil intensity; 4) the contribution of dust devils to atmospheric dust aerosols determined in East Asia was 30.4 ± 13%, thereby suggesting that dust devils contribute significantly to the total amount of atmospheric dust aerosols. Although the new parameterization scheme for dust devils was rough, it was helpful for understanding the distribution of dust devils and their contribution to the dust aerosol budget.

* Corresponding author. Collaborative Innovation Center on Forecast and Evaluation of Meteorological Disasters, Nanjing University of Information Science and Technology, Nanjing, 210044, China.
E-mail address: han-yx66@126.com (Y. Han).

https://doi.org/10.1016/j.atmosenv.2018.03.050
Received 23 August 2017; Received in revised form 20 March 2018; Accepted 22 March 2018
Available online 27 March 2018
1352-2310/ © 2018 Elsevier Ltd. All rights reserved.

1. Introduction

Dust aerosol is the most important constituent of aerosols, accounting for nearly half of the total aerosols in the troposphere (Lohmann and Feichter, 2005). It has significant impacts on global and regional climate via the "umbrella effect", "condensation effect" (Twomey et al., 1984; Albrecht, 1989; Huang et al., 2006), and "iron fertilizer effect" (Martin, 1990). Previous studies have shown that there is a significant negative correlation between dust concentration and global temperature in the Antarctic Vostok ice core, which suggests that a high dust concentration can lead to a low global carbon dioxide concentration, thereby resulting in global cooling (Ridgwell, 2002; Boyd et al., 2009; Maher et al., 2010). Through long-distance transmission, the dust aerosol from the continents is settled in the oceans and then reduces the global carbon dioxide concentration via the "iron fertilizer effect" to affect global climate (Overpeck et al., 1996; Ridgwell, 2002; Jickells et al., 2005). The decrease in global mean temperature of 2 °C–3 °C during the Little Ice Age was mainly dependent on the increased amount of dust aerosols, which had a significant impact on global cooling (Harvey, 1988).

Dust storms are an important dust emission mechanism mainly based on kinetics, and they have attracted the attention of many researchers due to their capacity to carry huge amounts of dust aerosols (Petit et al., 1999; Sokolik et al., 2001; Huebert et al., 2003; Zhao et al., 2008; Hahnenberger and Nicoll, 2012; Dagsson-Waldhauserova et al., 2013; Krasnov et al., 2016). However, the observed amount of global mineral dust is nearly 20 times larger than that simulated in ice ages (Maher and Dennis, 2001). Dust storms only occur rarely in the summer in northern China (Natsagdorja et al., 2003), so the mechanism responsible for dust storms cannot explain why the aerosol index observed by satellites is still very high in deserts (Deng et al., 2009). This fact implies that the total amount of dust aerosols in the atmosphere provided by dust storms may present an incomplete picture (Han et al., 2016).

Compared to the abundant studies on dynamic emission processes, the studies on the thermo-driven emissions are fewer and less robust. Small-scale processes, such as dust devils caused by thermodynamic emissions, can also lift dust aerosols into the atmosphere in the Gobi Desert region and over dry plowed fields (Koch and Renno, 2005). On sunny days with weak winds, solar radiation increases the ground sensible heat flux, causing the ground air temperature to rise; rising convection vortices will then form and carry dust aerosols into the atmosphere (Gu et al., 2010). Typical dust devils are generally 10 m in diameter with a typical duration of several minutes to an hour (Koch and Renno, 2005). The 2-m temperature difference between the inside and outside of dust devils is approximately 4 °C–8 °C, and the pressure difference is usually less than 2 hPa from the ambient air to the central part of dust devils (Tratt et al., 2003; Lorenz, 2013). Therefore, dust devils caused by thermal turbulence may be used to quantify the dust aerosols in non-dust storm seasons over deserts and adjacent areas.

Fieldwork pertaining to dust devils is very rare due to their sporadic appearance and fast mobility. The first series of focused investigations was conducted in the Avra Valley and the Tuscon basin in Arizona between 1960 and 1962 by Sinclair (1964, 1969). The output of Sinclair's research suggested that dust devil frequencies are suppressed when the wind speed exceeds a certain value and the temperature inside the dust devil is higher than the ambient air. They also found that dust devils are most likely to occur one to two hours after noon. The most important thing is that the basic parameter characteristics of the dust devils, such as the wind speed, pressure and temperature, were recorded. The observation by McGinnigle (1966) in northwest Libya focused on the influence of the soil on the dust devils. It was found to be more favorable for dust devil formation when the surface has a low thermal conductivity and a high thermal capacity with spatially uneven heating. The observation also noted the importance of low background winds for dust devil formation. Ryan (1972) found a strong correlation between the dust devil frequency and the lapse rate between 0.3 and 10 m above ground during a 30-day observation in the Mojave Desert, where approximately 250/km^2 of dust devils were recorded every day. Snow and McClelland (1990) validated the previous studies by conducting a field observation in New Mexico desert in 1986/1987. The field campaign found that dust devil occurrences and the peak of convective vortices had a significant correlation, and that the dust devils occur more often on flat and cleared areas and are modulated by sensible heat flux and surface property variations. It suggested that higher soil moisture may lead to a lower dust devil frequency. The impact of wind shear on dust devils was first quantified by Balme et al. (2003) during their observation in Eldorado Valley, Nevada. An empirical equation between the peak friction velocity and the peak tangential wind speed was given. Based on 557 dust devils observed in Australia, Oke et al. (2007) found that dust devils were restricted to ambient winds of 1.5–7 m s^{-1} with peak activity at 3 m s^{-1}, and a minimum lapse of ~0.9 K m^{-1} measured from 0.12 to 2.52 m above ground level was necessary to initiate dust devils.

Due to the difficulties in the direct observation of the basic characteristic parameters of dust devils, the quantification of such parameters still highly relies on the summaries of Ives (1947) and Sinclair (1973). The most advanced front of dust devil studies is model research. There are three basic types of models that may be applied to understand the formation of dust devils: 1) dynamic models; 2) thermodynamic models; 3) numerical models based on both the dynamic and the thermodynamic mechanisms. The dynamic model is suitable for vortex simulations (Kalashnik and Visheratin, 2010), but it fails to explain the impacts of the heat flux or the lapse rate on dust devil formation. The most fatal contradiction in the dynamic model is that it predicts an enhancement in the dust devil under strong winds (Rafkin et al., 2016), while in fact, dust devils are suppressed in high winds. The most accepted thermodynamic model is the heat engine theory, which attempts to interpret the dust devil as a system that converts heat into kinetic energy (Renno et al., 1998). Based on the original heat engine theory, the research of Lyons et al. (2008) considered dust devil intensity as a function of the surface pressure, the boundary layer height, the near-surface fraction coefficient, and the horizontal thermodynamic efficiency. The key factors for dust devil formation are the magnitudes of the convective buoyancy and rate of friction dissipation at the surface. A key criterion is proposed for the dust devil formation: the ratio of the convective velocity scale (w*) and the friction velocity (u*), marked as w*/u*, should be more than 5. However, the heat engine theory does not concern the mechanism of vortice formation; therefore, the source of vorticity for the dust devil is not explained by this theory (Rafkin et al., 2016). The large eddy simulation is one of the best species of the third class of model, which includes both the dynamic and thermodynamic mechanisms. After decades of improvement, the large eddy simulation is now able to capture the distribution of the meteorological factors inside a single dust devil. Dust devil formation requires vertical vortices and strong updrafts, which are caused by horizontal wind shear and a sufficiently large temperature lapse rate originating from solar radiation, respectively (Cortese and Balachandar, 1993; Shapiro and Kogan, 1994; Kanak et al., 2000, 2005; Leovy, 2003; Toigo, 2003; Gu et al., 2008; Zhao et al., 2008; Gu et al., 2010; Fujiwara et al., 2011; Ito et al., 2013; Klose and Shao, 2013). Furthermore, the large eddy simulation considers the tilt of horizontal convective vortices (Hess and Spillane, 1990) and the mixing of convective bubbles (Carroll and Ryan, 1970) as important mechanisms to initiate a dust devil. Although the results of the large eddy simulation still differ significantly from the observational data, they provide an insight into dust devil formation (Leovy, 2003). With the exception of the large eddy simulation, the WRF model has been adopted to simulate the regional or global distribution of dust devils. By taking the large eddy simulation model in WRF, coupled with the critical parameters for dust devil formation, Klose and Shao (2013) managed to simulate the spatial distribution of dust devils in Australia and calculated their contribution to the total

dust aerosols. By employing the three key criteria for dust devil formation—background wind speed less than 7 m s^{-1} (Oke et al., 2007), w*/u* > 5.0 (Lyons et al., 2008), and a lapse rate between 0 and 2 m more than 8.5 K m^{-1} (Ansmann et al., 2009)—the simulation by Jemmett-Smith et al. (2015) used data from the European Centre for Medium-Range Weather Forecasts (ECMWF) to quantitatively estimate the dust devil regions around the world. The simulated regions where dust devils are frequently captured mainly lie in West Africa, Southwest South Africa, Southwest USA, the Red Sea coast of the Arabian Peninsula, Northwestern China, the west coast of South America, and Australia.

The potential for dust devil emissions determines their contribution to the atmospheric dust aerosol budget. Research into dust devils is comparatively scarce, so there is no accurate method for calculating the potential total dust devil emissions. In the continental USA, approximately 65% of the dust aerosols come from dust devils (Gillette and Sinclair, 1990). In addition, dust devils contribute closely 35% to the global dust aerosol budget (Koch and Renno, 2005). In particular, the Sahara Desert may provide more than 30% of the total amount of global dust devil emissions (Marsham et al., 2008). Thus, dust devils comprise an important component of the global dust aerosol. However, based on high-resolution operational data, Jemmett-Smith et al. (2015) indicated that dust devils can deliver approximately 7.29 × 10^7 t of dust aerosols per year into the atmosphere, which only accounts for approximately 3.4% of the global dust aerosols. This proportion is only 1/10th of the amount reported by Koch and Renno (2005) and Han et al. (2016), and it is also inconsistent with indirect observations. These large fluctuations in the simulation results demonstrate the significant uncertainty that affects dust devil simulations. Thus, further research is needed to determine whether dust devils play an important role in local dust emissions.

In the present study, we performed a simulation using WRF-Chem (Weather Research and Forecasting model coupled with Chemistry) (Grell et al., 2005; Fast et al., 2006; Skamarock et al., 2008) and coupled it with a new parameterization scheme for dust devils in order to determine the temporal and spatial distribution characteristics of dust devils and the contribution of dust devils to the dust aerosol budget in East Asia.

2. Study area, methods and a new parameterization scheme for dust devils

2.1. Study area

The study area was mainly located in northwest China. The region covered Taklimakan, Gurbantunggut, Kumtag, Badain Jaran, Tengger, Ulan Buh, Hobq, Mu Us, Onqin Daga, Horqin, and Qaidam, forming an east-west mid-latitude desert belt (Fig. 1). The desert area covered 1.5 × 10^6 km^2, which was approximately 15.9% of the land area in China (Sun et al., 1998). To simplify the following description, Badain Jaran, Tengger, Ulan Buh, Hobq, and Mu Us are referred to as BTUHM.

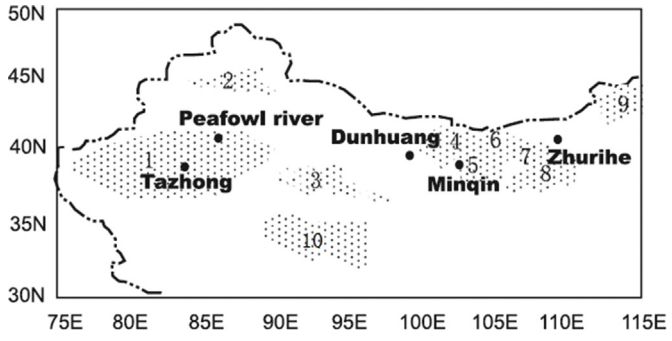

Fig. 1. Distribution of deserts and location of observation stations in East Asia. Note: 1. Taklimakan; 2. Gurbantunggut; 3. Kumtag; 4. Badain Jaran; 5. Tengger; 6. Ulan Buh; 7. Hobq; 8. Mu Us; 9. Onqin Daga; 10. Qaidam.

Table 1
Main physical schemes used in WRF-Chem.

Physical Scheme	
Cloud microphysics scheme	Lin (Lin et al., 1983)
Planetary boundary layer scheme	YSU (Hong et al., 2006)
Land-surface scheme	Noah (Ek et al., 2003)
Surface layer scheme	Monin-Obukhov (Obukhov, 1971)
Short wave radiation	RRTMG (Mlawer et al., 1997; Iacono et al., 2000)
Long wave radiation	
Dust source mask	Dust source function S (Ginoux et al., 2001)
Dust storm emission	Shao scheme (Shao, 2001)

2.2. Model description

WRF-Chem was used to simulate the meteorological processes and the aerosol cycle over East Asia in 2009. A model domain with 222 × 184 grids and a horizontal grid spacing of 30 km was employed, where 33 vertical layers extended from the ground to 10 hPa. The initial and boundary meteorological conditions were derived from the National Centers for Environmental Prediction Final Analysis data, where the length of the integration period was from January to December 2009, and the temporal resolution was 120 s. The spin-up time was set to 30 days. To estimate the contribution of dust devils to the atmospheric dust aerosol budget, the emissions from dust storms are also required. The dust storm emission scheme from Shao (2001) is adopted in the simulation, which has been proven to have high accuracy in simulating the characteristics of dust in East Asia (Wu and Lin, 2014). The main physical schemes used are shown in Table 1.

2.3. A new parameterization scheme for dust devils

There was no existing parameterization scheme for dust devils in WRF-Chem, so a new parameterization scheme for dust devils was established. It mainly consists of two parts:

The weather criteria for dust devil formation: (1) The ratio of the availability of convective buoyancy, w_*, relative to frictional dissipation, u_*, should be greater than 5 (Lyons et al., 2008); (2) The LR, defined as the temperature drop per unit height, should be from 8.5 to 10 K m^{-1} in the near-surface level (0–2 m) (Ansmann et al., 2009; Jemmett-Smith et al., 2015); (3) Wind speed should be between 2 and 7 m s^{-1} (Ansmann et al., 2009; Oke et al., 2007).

The dust devil emission: The simple thermodynamic theory for dust devils proposed by Renno et al. (1998) states that the total dust devil emission (DAE_{tot}) depends on the thermodynamic efficiency:

$$DAE_{tot} = S \times \sigma \times F_d, \quad (1)$$

where F_d is the estimated average dust flux in a dust devil flux of 0.7 g m^{-2} s^{-1} (Koch and Renno, 2005), S is the grid area where the dust devil's instantaneous position is located (Sinclair, 1969; Balme and Greeley, 2006; Oke et al., 2007), and each grid area measures 9 × 10^8 m^2. The fractional area σ (Koch and Renno, 2005) covered by a dust devil is estimated by:

$$\sigma \approx \left(\frac{\mu}{\eta}\right)^{\frac{1}{2}} \left(\frac{\Delta p}{\rho_{air} g T_R}\right)^{\frac{3}{2}} \left(\frac{F_{in}}{\rho_{air}}\right)^{-\frac{1}{2}}, \quad (2)$$

where μ is the dimensionless coefficient for the turbulent dissipation of mechanical energy within 12–24, and the pressure difference from the surface to the convection boundary layer is $\Delta p = \rho_{air} g Z_{CBL}$. The air density ρ_{air} is 1 kg m^{-3}, the acceleration due to gravity g is 9.8 g m^{-2}, F_{in} is the heat input into the convective heat engine, F_{in} = 11 ± 5 kW m^{-2}, and the radiative timescale of the convective boundary layer T_R is 9 × 10^5 s. The thermodynamic efficiency η is

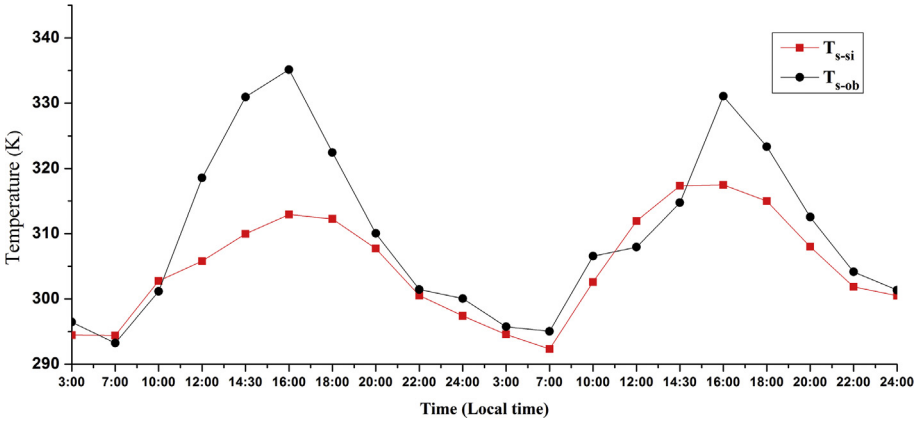

Fig. 2. Surface temperature at Central Taklimakan meteorological station (39°N, 83.4°E) (Jul 21–22, 1987).

estimated by:

$$\eta = \frac{\Gamma_{ad} Z_{CBL}}{T_h}, \quad (3)$$

where Z_{CBL} is the height of the convection boundary layer, T_h is the surface temperature, and Γ_{ad} is the adiabatic LR ($\Gamma_{ad} = 10\,K\,km^{-1}$).

2.4. Improvement of the LR threshold in East Asia

The LR threshold for dust devil formation was an important factor. However, the WRF-Chem simulated surface temperature ($T_{s\text{-}si}$) was often lower compared to the observed surface temperature ($T_{s\text{-}ob}$) in East Asian deserts. For example, at Central Taklimakan meteorological station (39°N, 83.4°E) during July 21–22, 1987 (Li, 2003), $T_{s\text{-}si}$ was significantly (10 K–20 K) lower than $T_{s\text{-}ob}$ in the daytime, while the difference was not large at night (Fig. 2). A similar underestimation also appears at the Dunhuang meteorological station (40.1°N, 94.31°E) (January, April, July, and October in 2009) (Wang et al., 2011). Fig. 3 shows that during the 4-month period, the trend of LR_{si} matched well with that of LR_{ob}, but its values were substantially smaller. The maximum underestimation was approximately 2.5 K m^{-1} in January, 2.5–5 K m^{-1} in April and October, and 5–7.5 K m^{-1} in July. LR was underestimated mainly because of the underestimated $T_{s\text{-}si}$ in the summer (Fig. 4) (Wang et al., 2011), since the simulated 2-m air temperature ($T_{2m\text{-}si}$) was slightly lower than the observed temperature ($T_{2m\text{-}ob}$) in the daytime, but $T_{s\text{-}si}$ was 5–15 K lower than $T_{s\text{-}ob}$.

In summary, LR_{si} was 2.5–7.5 K m^{-1} lower than LR_{ob} in East Asia in summer afternoons. Considering that LR_{si} is underestimated by nearly 5 K m^{-1}, the LR threshold should be reduced to 3.5–5 K m^{-1}. In this paper, the LR threshold was adjusted to 4 K m^{-1} due to this underestimation, which plays the equivalent role to the 8 K m^{-1} threshold in other studies (Ansmann et al., 2009; Jemmett-Smith et al., 2015).

3. Results

3.1. Simulation of the temporal and spatial variation of dust devils

3.1.1. The diurnal temporal variation

To analyze the diurnal and monthly variations in dust devils, we selected Taklimakan as a representative region. Fig. 5 shows that the monthly averaged diurnal variations in the dust devil emissions in Taklimakan had unimodal distributions. In general, the dust devils began to occur around 08:00–09:00 h (local time) and increased rapidly from 10:00 to 14:00 h, reaching a peak at approximately 14:00–16:00 h, and then decreasing sharply. After 18:00 h, the emissions of dust devils were almost negligible. The peak was lower and the lasting period was

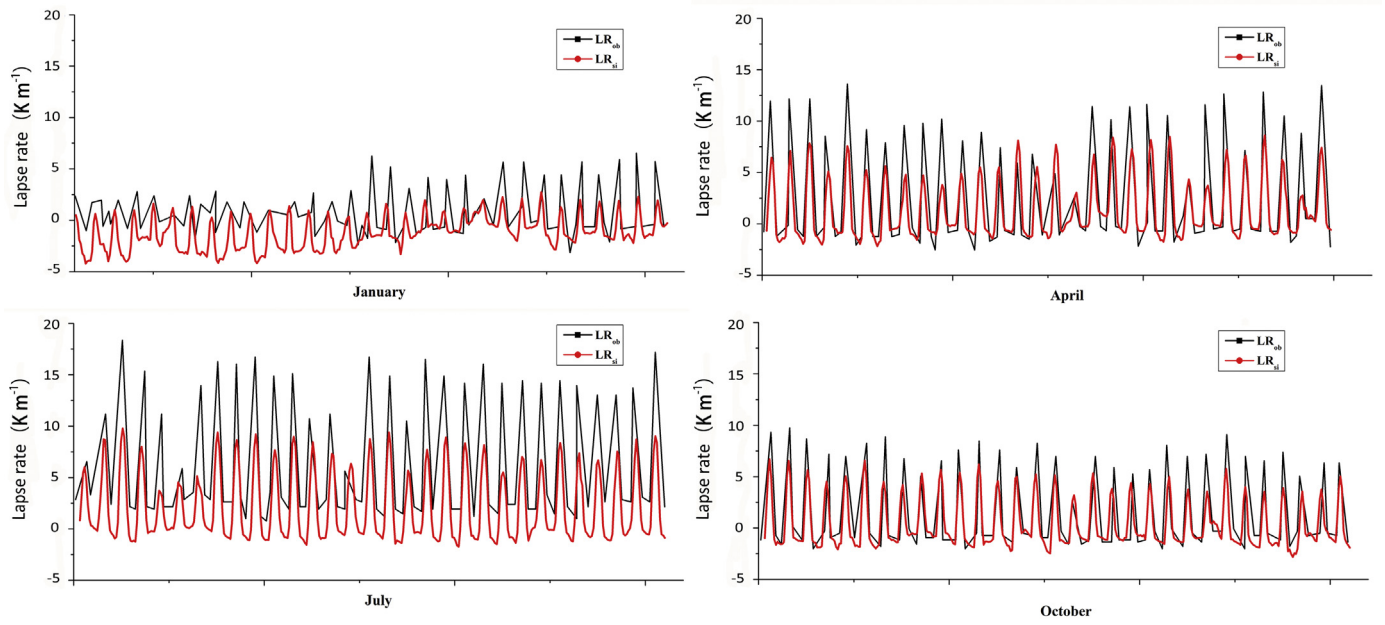

Fig. 3. Diurnal variation in LR in January, April, July, and October in 2009 at Dunhuang.

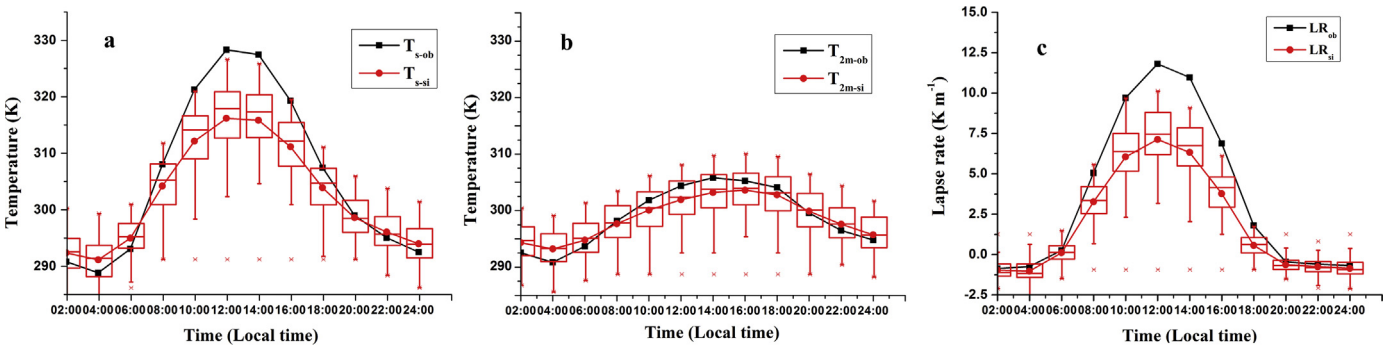

Fig. 4. Monthly mean diurnal variation in the surface temperature (a), the 2-m air temperature (b) and LR (c) during the summer of 2009 at Dunhuang.

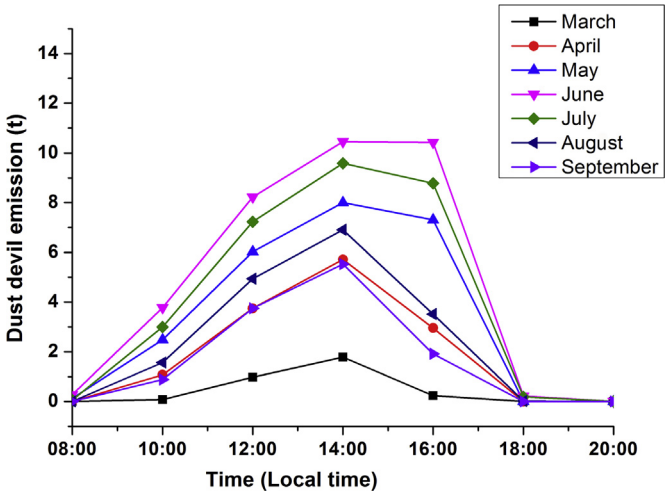

Fig. 5. Variation in simulated monthly mean diurnal dust devil emissions in Taklimakan.

shorter in March, April, August and September, whereas the maximum emissions occurred in June and July.

The observed diurnal mean dust devil frequency was derived from the Peacock River in Taklimakan (Fig. 6a), and the diurnal mean extinction coefficient was obtained by using LIDAR in Minqin, BTUHM (Fig. 6b) (Le, 1983; Han et al., 2016). The trends of mean frequency (Fig. 6a) and mean extinction coefficient (Fig. 6b) of dust devils were almost uniform. The simulated mean dust emission curve (Fig. 6a) had broadly the same tendency, which indicated that the simulation was reliable. At the same time, the standard deviation of the simulated diurnal dust devil emissions (from March to September) increased gradually after 8:00 h, reaching the peak at 16:00 h, then decreased sharply, almost reaching 0 at 18:00 h. The median of the diurnal dust devil emissions was nearly the same as the mean, only slightly lower at 16:00 h.

3.1.2. Diurnal spatial distribution and intensity

Sunny days provide favorable conditions for dust devil formation, so the diurnal distribution of dust devils was simulated for June 12, 2009. The time difference is approximately 2 h from the east of BTUHM to the west of Taklimakan due to the long distance. Using Beijing Time (GMT + 8), Fig. 7 shows that BTUHM and the southern part of Mongolia had small sporadic dust devils at approximately 10:00 h. After 12:00 h, the dust devils extended northward and westward in BTUHM as well as occurring in Taklimakan and Kumutag. From 14:00 to 16:00 h, dust devils covered nearly all of North China, where the maximum was reached at 16:00 h. At 18:00 h, the region in BTUHM with dust devils began to contract, and they almost disappeared from East Asia after 20:00 h.

The intensity of the dust devils was calculated according to Equation (2). The distribution of the dust devils changed in different periods. However, the fractional area σ depends on the surface temperature and boundary layer height, so the intensity of dust devils also exhibited a new feature. At approximately 10:00 h, BTUHM had a fragmented dust devil distribution of below 18 $\mu g\, m^{-2}$. At 12:00 h, the intensity in BTUHM increased to 21 $\mu g\, m^{-2}$, with another high value area at the center of Taklimakan, although its magnitude and scope were less than those in BTUHM. At 14:00–16:00 h, the intensity in the two desert areas increased to 24 $\mu g\, m^{-2}$ or more. However, the emissions in BTUHM disappeared at 18:00 h, whereas a high value area still

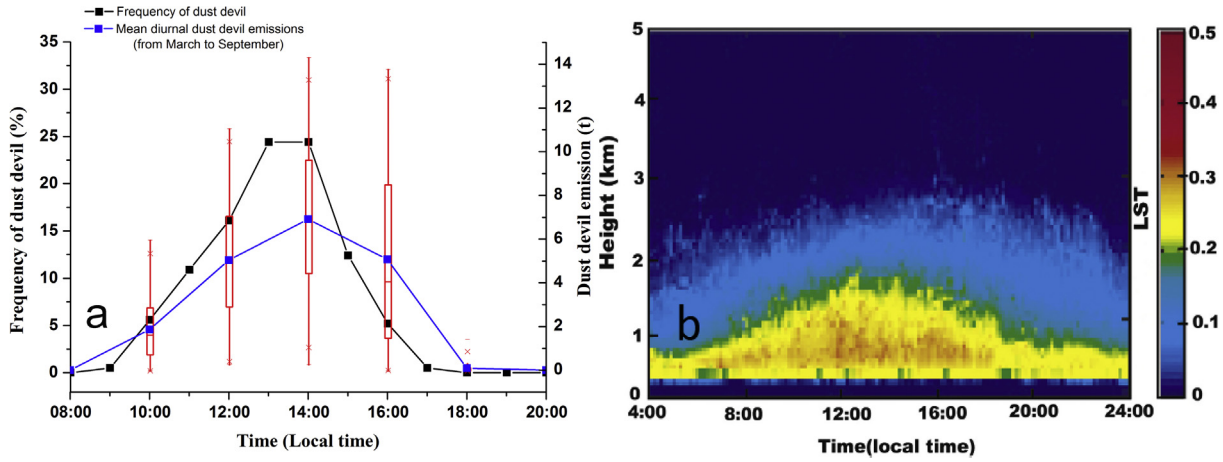

Fig. 6. Observed mean diurnal dust devil frequency at Peacock River from 1964 to 1970, the variation in simulated mean diurnal dust devil emissions in Taklimakan (a), and the observed diurnal mean extinction coefficient at Minqin during April 2008 (b).

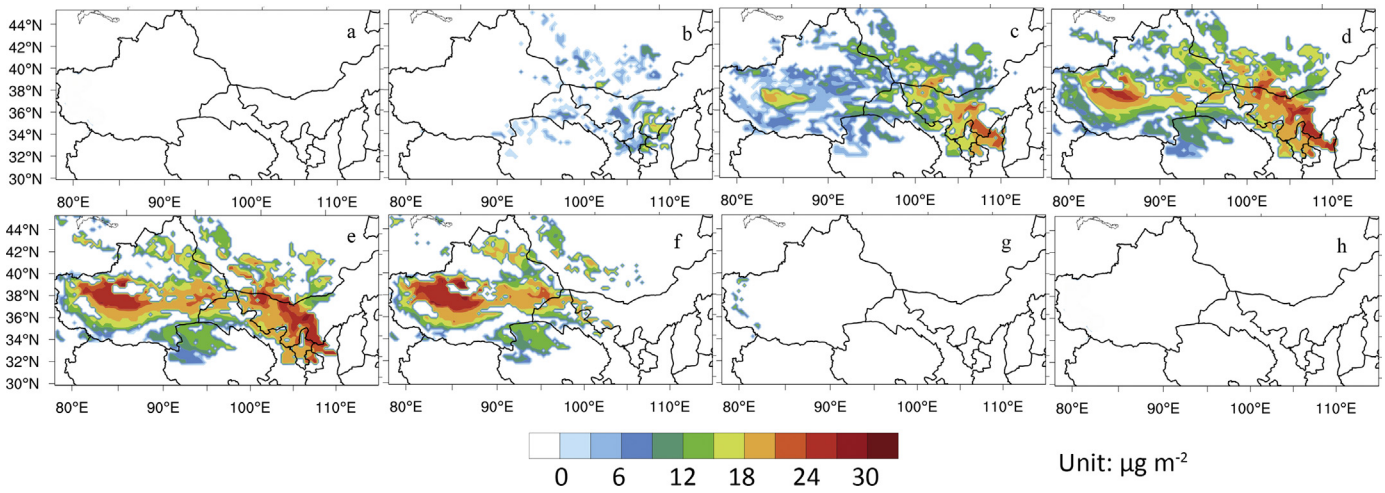

Fig. 7. Simulated diurnal spatial distribution and intensity of dust devils (Jun 12, 2009) (a: 8:00; b: 10:00; c: 12:00; d: 14:00; e: 16:00; f: 18:00; g: 20:00; h: 22:00).

existed in Taklimakan; however, it decreased to 0 at 20:00 h.

In general, the distribution and center of intensity of the dust devils gradually shifted with time from east to west, where the earliest dust devil area appeared in the eastern desert (BTUHM).

3.1.3. Monthly temporal and spatial distribution and intensity

Fig. 8 shows the distribution and intensity of dust devils in East Asia between April and September 2009. Virtually no dust devil emissions occurred between October and March in the following year. During April, the distribution area of dust devils expanded rapidly, mainly in Taklimakan, Kumutag, and Qaidam, where the emissions increased to 400–800 $\mu g\, m^{-2}$. During May, the dust devils extended to all of the deserts in East Asia, and the emissions also increased rapidly. In the middle of Taklimakan, the dust devil emissions reached 1000–1400 $\mu g\, m^{-2}$, while the emissions were approximately 800–1000 $\mu g\, m^{-2}$ in Kumutag and Qaidam. During June, the distribution of dust devils was similar to that in May, and the maximum intensity occurred. The region with maximum emissions was in Taklimakan, where the levels exceeded 1800 $\mu g\, m^{-2}$, while the emissions in Kumutag and Qaidam increased to 1000–1400 $\mu g\, m^{-2}$. In addition, a new high value area appeared in the BTUHM, where the emissions were approximately 1000–1400 $\mu g\, m^{-2}$. During July, the dust devil distribution was similar to that in May and June, but the emissions began to decline, where the total emissions from each desert were less than those in June but greater than those in May. During August, the total emissions from each desert continued to decline, where the intensity and distributions in different areas were similar to those in April. The dust devil areas began to contract in September, and the emissions were also less than those in April, then disappeared in October until March in the following year.

Taklimakan was selected to illustrate the monthly variations in dust devils (Fig. 9). Dust devils appeared from February to March, and the emissions remained at a low level. The dust devils increased rapidly in April and reached a peak in mid-June, before gradually decreasing. The dust devil emissions finished by the middle of November. The simulated unimodal curve was consistent with the trends of mean frequency of the observed dust devils at Peacock River (Le, 1983).

3.2. Analysis of an example about the changes in the distribution and intensity of dust devils

Figs. 7–8 show that the distribution and intensity of dust devils changed with time in each grid depending on whether the grids fit the favorable weather criteria for dust devil formation: LR > 4 K m^{-1}, w_*/

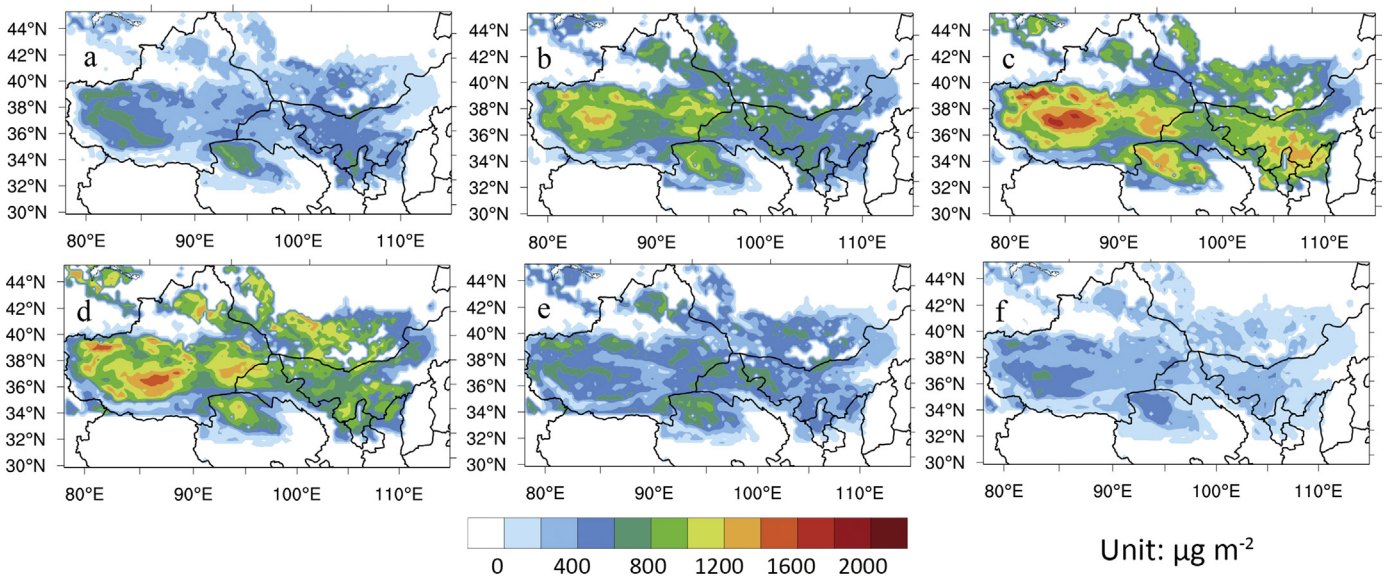

Fig. 8. Simulated monthly distribution and intensity of dust devils in 2009 (a: April; b: May; c: June; d: July; e: August; f: September).

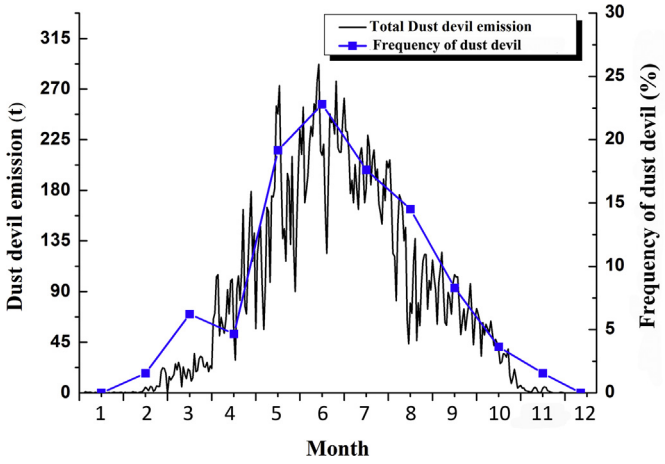

Fig. 9. Monthly variations in dust devils (black: simulated diurnal total dust devil emissions at Taklimakan; blue: observations at Peacock River). (For interpretation of the references to colour in this figure legend, the reader is referred to the Web version of this article.)

$u_* > 5$, and wind speed = 2–7 m s^{-1}. According to their monthly variation in June, for example, the average LR was greater than 4 K m^{-1} in most of the desert area, but lower than 4 K m^{-1} in BTUHM (Fig. 10a); the average wind speed in each desert fit well with the threshold for dust devils (Fig. 10b), and w_*/u_* was greater than 5 in Taklimakan and some scattered areas distributed sporadically (Fig. 10c). In the study area, dust devils were assumed to appear in the grids where all three criteria above were satisfied. After determining the positions of dust devils, according to Equation (3), the intensity of dust devils was mainly affected by T_s and the boundary layer height. According to Fig. 10d, a high value belt of T_s stretched from Taklimakan to BTUHM and covered most of the high dust devil frequency area. The average T_s across the belt was above 305 K, whereas it exceeded 310 K in Taklimakan. The boundary layer heights in Taklimakan and BTUHM ranged between 2100 and 2400 m (Fig. 10e). As a result, intense dust devils mainly occurred in the desert area, especially Taklimakan, because the weather criteria for dust devil formation and the affecting factors for dust devil intensity are better satisfied there.

3.3. Estimated dust devil emissions in East Asia

The instantaneous dust devil emissions in the study area were integrated with a time step of seconds, and the grids were then added together to obtain the total amount of dust devil emissions. In 2009, the estimated total dust devil emissions in East Asia comprised 4.6×10^7 t. By applying the dust storm scheme in the model, the dust storm emission can be obtained during the model run. The dust storm emission amount is given as 11.8×10^7 t. Compared with the annual mean dust storm emissions recorded in other simulations with roughly the same study area as in this study (5.4×10^7 t (Werner et al., 2002), 5×10^7 t (Miller et al., 2004), 21.4×10^7 t (Tanaka and Chiba, 2006), 4.82×10^7 t (Liu et al., 2013), and 14.6×10^7 t (Liu et al., 2015)), it is appropriate in magnitude. The dust storm emissions simulated by different numerical models were generally between 4.82×10^7 t and 21.4×10^7 t, and the average was 10.5×10^7 t. After adding the average emission by dust storms to the total emission of dust devils, the total amount of atmospheric dust was calculated as $15.1 \times 10^7 \pm 6.72 \times 10^7$ t. The contribution of dust devils to the atmospheric dust aerosol budget in East Asia was 30.4 ± 13%, lower than the 52% contribution in Taklimakan calculated by Han et al. (2016), yet consistent with the conclusions of Koch and Renno (2005). Therefore, the dust devils made a great contribution to the atmospheric dust aerosol budget.

4. Conclusion

In the present study, we used the WRF-Chem model and National Centers for Environmental Prediction Final Analysis data to simulate the diurnal and monthly characteristics of dust devils in East Asia, and we then estimated the contribution of dust devils to the total amount of atmospheric dust aerosols in East Asia. Our results can be summarized as follows:

1) A new parameterization scheme for dust devils was established. It mainly consists of two parts: the weather criteria for dust devil formation and the dust devil emission. Coupled with WRF-Chem, it can simulate the temporal distribution and the speculated cursory spatial characteristics of dust devils.
2) The simulated diurnal and monthly variations in dust devil emissions had unimodal distributions. The dust devil emissions were relatively low in the morning, but they increased rapidly during

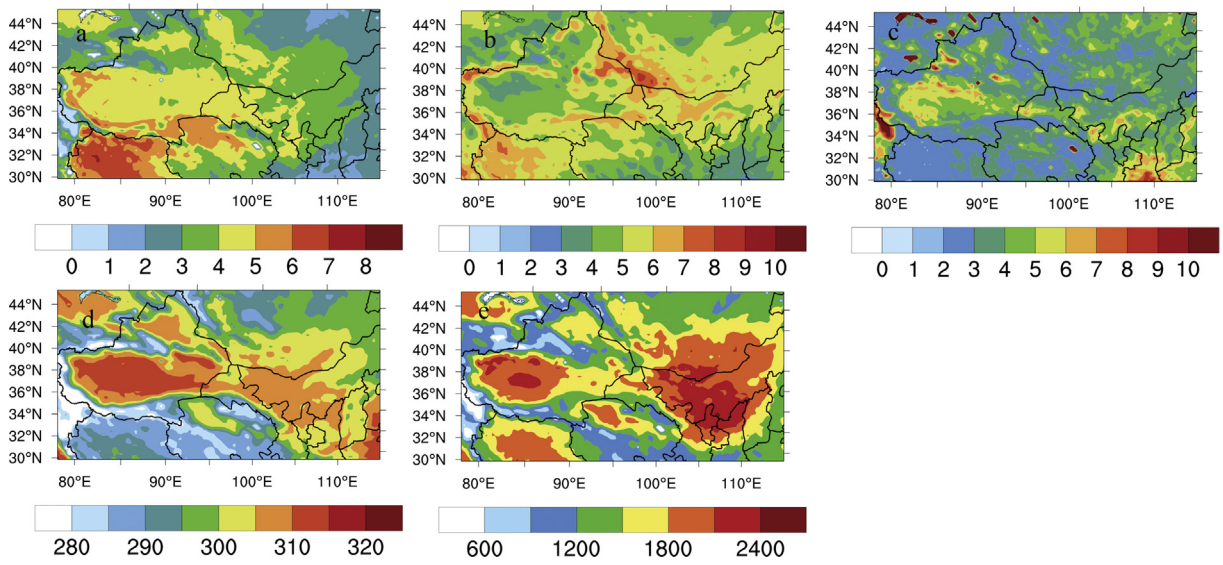

Fig. 10. Simulated weather criteria that govern the distribution and intensity of dust devils in June 2009 (a: LR (K m^{-1}); b: wind speed (m s^{-1}); c: w*/u*; d: surface temperature (K); and e: boundary layer height (m)).

10:00–14:00 h before reaching a peak in the afternoon and then decreasing quickly, with almost no emissions by approximately 20:00 h. Dust devils appeared from March, and their frequency increased rapidly in April before reaching a peak in mid-June. Then, they gradually decreased and disappeared by mid-November, where the simulated variations were similar to the observed diurnal and monthly variations.

3) Simulated dust devils appeared frequently in deserts, including the Gobi, where the distribution and intensity of dust devils was highest in the afternoon. The distributed area and the center of intensity of the dust devil moved from east to west during the day. The monthly spatial distribution was different from the diurnal distribution. Dust devils began appeared sporadically in March, while the intensity and distribution peaked in June, and dust devils hardly occurred in East Asia since October.
4) Three criteria that govern the formation of dust devils should be satisfied at the same time: LR $> 4\,K\,m^{-1}$, $w_*/u_* > 5$, and wind speed = 2–7 $m\,s^{-1}$. In most desert areas, the LR and wind speed can satisfy the thresholds, but the grids where w_*/u_* exceeded the threshold existed mainly in Taklimakan, and only sporadically in other deserts. Thus, the main limiting factor for dust devil formation in East Asia is w_*/u_*. The intensity of dust devils is determined by the existence of the dust devil, T_s, and the boundary layer height.
5) The estimated total dust devil emissions in East Asia comprised 4.6×10^7 t in 2009, which contributed 30.4 ± 13% to the atmospheric dust aerosol budget in East Asia. These results suggest that dust devils contribute significantly to the atmospheric dust aerosol budget.

The temporal and spatial distribution of dust devils is determined according to the new parameterization scheme for dust devils, which matches the results of Le (1983): the dust devils mainly tend to occur in the deserts and Gobi at noon. However, there hardly exists any large-scale observation record of dust devils, thus the simulation conclusions about dust devils still need further confirmation by observations. It is worth noting that no dust devils were predicted by the simulation from November to February in the following year, which does not agree with the observations (Le, 1983). Such a fact indicates that there are some defects in the current parameterization scheme for dust devils. For example, the wind speed is assumed to be 2–7 $m\,s^{-1}$ in the present scheme, whereas some studies suggest that a dust devil is more likely to form under calm wind or weak wind (Hess and Spillane, 1990; Toigo, 2003). In addition, the scheme does not consider the surface wind stress caused by horizontal differences in the surface temperature, which originate from uneven surface heating. Many other mechanisms related to dust devil formation are still not included in the model, and thus further research is required.

Acknowledgments

This study has been co-supported by the National Natural Science Foundation of China (41375158). Two anonymous reviewers are appreciated for their valuable comments.

References

Albrecht, B.A., 1989. Aerosols, cloud microphysics, and fractional cloudiness. Science 245, 1227–1230.
Ansmann, A., Tesche, M., Knippertz, P., Bierwirth, E., Althausen, D., Müller, D., Schulz, O., 2009. Vertical profiling of convective dust plumes in southern Morocco during SAMUM. Tellus, Ser. B 61, 340–353.
Balme, M., Greeley, R., 2006. Dust devils on Earth and Mars. Rev. Geophys. 44 (3), 1–22 RG3003.
Balme, S. Metzger, Towner, M., Ringrose, T., Greeley, R., Iversen, J., 2003. Friction wind speeds in dust devils: a field study. Geophys. Res. Lett. 30 (16). http://dx.doi.org/10.1029/2003JE002096.
Boyd, P.W., Mackie, D.S., Hunter, K.A., 2009. Aerosol iron deposition to the surface ocean-Modes of iron supply and biological responses. Mar. Chem. 120 (1), 128–143.
Carroll, J.J., Ryan, J.A., 1970. Atmospheric vorticity and dust devil rotation. J. Geophys. Res. 75 (27), 5179–5184.
Cortese, T., Balachandar, S., 1993. Vortical nature of thermal plumes in turbulent convection. Phys. Fluid. A Fluid Dynam. 5 (12), 3226–3232.
Dagsson-Waldhauserova, P., Arnalds, O., Olafsson, H., 2013. Long-term frequency and characteristics of dust storm events in Northeast Iceland (1949-2011). Atmos. Environ. 77 (7), 117–127.
Deng, Z.Q., Han, Y.X., Bai, H.Z., Zhao, T.L., 2009. Reason analysis of the dust aerosols' content change in desert regions. China Environ. Sci. (Chin.) 29 (12), 1233–1238.
Ek, M.B., Mitchell, K.E., Lin, Y., Rogers, E., Grunmann, P., Koren, V., Gayno, G., Tarpley, J.D., 2003. Implementation of Noah land surface model advances in the National Centers for Environmental Prediction operational mesoscale Eta model. J. Geophys. Res. 108 (D22), 8851. http://dx.doi.org/10.1029/2002JD003296.
Fast, J.D., Gustafson Jr., W.I., Easter, R.C., Zaveri, R.A., Barnard, J.C., Chapman, E.G., Grell, G.A., 2006. Evolution of ozone, particulates, and aerosol direct forcing in an urban area using anew fully-coupled meteorology, chemistry, and aerosol model. J. Geophys. Res. 111, D21305. http://dx.doi.org/10.1029/2005JD006721.
Fujiwara, C., Yamashita, K., Nakanishi, M., Fujiyoshi, Y., 2011. Dust devil-like vortices in an urban area detected by a 3D scanning Doppler lidar. J. Appl. Meteorol. Climatol. 50 (3), 534–547. http://dx.doi.org/10.1175/2010JAMC2481.1.
Gillette, D., Sinclair, P.C., 1990. Estimation of suspension of alkaline material by dust devils in the United States. Atmos. Environ. 24, 1135–1142.
Ginoux, P., Chin, M., Tegen, I., Prospero, M., Holben, B., Dubovic, O., Lin, S.J., 2001. Sources and distributions of dust aerosols simulated with the GOCART model. J. Geophys. Res. 106, 20,255–20,273. http://dx.doi.org/10.1029/2000JD000053.
Grell, G.A., Peckham, S.E., Schmitz, R., McKeen, S.A., Frost, G., Skamarock, W.C., Eder, B., 2005. Fully coupled "online" chemistry within the WRF model. Atmos. Environ. 39 (37), 6957–6975.
Gu, Z.L., Qiu, J., Zhao, Y.Z., Li, Y., 2008. Simulation of terrestrial dust devil patterns. Adv. Atmos. Sci. 25, 31–42.
Gu, Z.L., Wei, W., Zhao, Y.Z., 2010. An overview of surface conditions in numerical simulations of dust devils and the consequent near-surface air flow fields. Aerosol Air Qual. Res. 10, 272–281.
Hahnenberger, M., Nicoll, K., 2012. Meteorological characteristics of dust storm events in the eastern Great Basin of Utah, USA. Atmos. Environ. 60 (11), 601–612.
Han, Y.X., Wang, K.H., Liu, F., Zhao, T.L., Yin, Y., Duan, J.P., Luan, Z.P., 2016. The contribution of dust devils and dusty plumes to the aerosol budget in western China. Atmos. Environ. 126, 21–27.
Harvey, L.D.D., 1988. Climatic impact of ice age aerosols. Nature 334, 333–335.
Hess, G., Spillane, K., 1990. Characteristics of dust devils in Australia. J. Appl. Meteorol. 29 (6), 498–507.
Hong, S.Y., Noh, Y., Dudhia, J., 2006. A new vertical diffusion package with an explicit treatment of entrainment processes. Mon. Weather Rev. 134 (9), 2318–2341.
Huang, J.P., Minnis, P., Lin, B., Wang, T.H., Yi, Y.H., Hu, Y.X., Sun-Mack, S., Ayers, K., 2006. Possible influences of Asian dust aerosols on cloud properties and radiative forcing observed from MODIS and CERES. Geophys. Res. Lett. 33, L06824. http://dx.doi.org/10.1029/2005GL024724.
Huebert, B.J., Bates, T., Russell, P.B., Shi, G., Kim, Y.J., Kawamura, K., Carmicheal, G., Nakajima, T., 2003. An overview of ACE-Asia: strategies for quantifying the relationships between Asian aerosols and their climatic impacts. J. Geophys. Res. 108 (D23), 8633. http://dx.doi.org/10.29/2003JD003550.
Iacono, M.J., Mlawer, E.J., Clough, S.A., Morcrette, J.-J., 2000. Impact of an improved longwave radiation model, RRTM, on the energy budget and thermodynamic properties of the NCAR community climate mode, CCM3. J. Geophys. Res. 105, 14873–14890.
Ito, J., Niino, H., Nakanishi, M., 2013. Formation mechanism of dust devil-like vortices in idealized convective mixed layers. J. Atmos. Sci. 70 (4), 1173–1186. http://dx.doi.org/10.1175/JAS-D-12-085.1.
Ives, R.L., 1947. Behavior of dust devils. Bull. Am. Meteorol. Soc. 28, 168–174.
Jemmett-Smith, B.C., Marsham, J.H., Knippertz, P., Gilkeson, C.A., 2015. Quantifying global dust devil occurrence from meteorological analyses. Geophys. Res. Lett. 42, 1275–1282. http://dx.doi.org/10.1002/2015GL063078.
Jickells, T.D., An, Z.S., Andersen, K.K., Baker, A.R., Bergametti, G., Brooks, N., Cao, J.J., Boyd, P.W., Duce, R.A., Hunter, K.A., Kawahata, H., Kubilay, N., laRoche, J., Liss, P.S., Mahowald, N., Prospero, J.M., Ridgwell, A.J., Tegen, I., Torres, R., 2005. Global iron connections between desert dust, ocean biogeochemistry, and climate. Science 308 (5718), 67–71.
Kalashnik, K.N., Visheratin, 2010. Cyclostrophic adjustment and nonlinear oscillations in the core of an intense atmospheric vortex. Izvestiya Atmos. Ocean. Phys. 46 (5), 591–596.
Kanak, K.M., 2005. Large eddy simulation of coherent structures and dust devil-like vortices in the martian boundary layer. Lunar Planet Sci. Conf. 36.
Kanak, K.M., Lilly, D.K., Snow, J.T., 2000. The formation of vertical Vortices in the convective boundary layer. Q. J. R. Meteorol. Soc. 126 (569), 2789–2810.
Klose, M., Shao, Y., 2013. Large-eddy simulation of turbulent dust emission. Aeolian Res. 8, 49–58. http://dx.doi.org/10.1016/j.aeolia.2012.10.010.
Koch, J., Renno, N.O., 2005. The role of convective plumes and vortices on the global aerosol budget. Geophys. Res. Lett. 32, L18806. http://dx.doi.org/10.1029/2005GL023420.
Krasnov, H., Katra, I., Friger, M., 2016. Increase in dust storm related PM10 concentrations: a time series analysis of 2001-2015. Environ. Pollut. 213, 36.
Le, Z., 1983. The dust devils on the south Gobi of Xinjiang. Meteorol. (Chin.). Mon. 4, 33.
Leovy, C.B., 2003. Mars: the devil is in the dust. Nature 424 (6952), 1008–1009.
Li, J.F., 2003. Climate in Taklimakan Desert and Surrounding Mountains. Science Press (Chinese).
Lin, Y.L., Farley, R.D., Orville, H.D., 1983. Bulk parameterization of the snow field in a

cloud model. J. Clim. Appl. Meteorol. 22 (6), 1065–1092.
Liu, J.H., Zhao, T.L., Han, Y.X., Gong, S.L., Xiong, J., 2013. Modeling study on distributions and variations of global dust aerosol sources and sinks. China Environ. Sci. (Chin.) 33 (10), 1741–1750.
Liu, C., Zhao, T.L., Xiong, J., Liu, Y., Han, Y.X., Liu, F., 2015. A simulated climatology of dust aerosol emissions over 1991-2010 and the influencing factors of atmospheric circulation over the major deserts in the world. J. Desert Res. 35 (4), 959–970.
Lohmann, U., Feichter, J., 2005. Global indirect aerosol effects: a review. Atmos. Chem. Phys. 5 (3), 715–737.
Lorenz, R.D., 2013. Irregular dust devil pressure drops on Earth and Mars: effect of cycloidal tracks. Planet. Space Sci. 76, 96–103.
Lyons, T.J., Nair, U.S., Foster, I.J., 2008. Clearing enhances dust devil formation. J. Arid Environ. 72, 1918–1928.
Maher, B.A., Dennis, P.E., 2001. Evidence against dust-mediated control of glacial-interglacial changes in atmospheric CO2. Nature 410, 176–180.
Maher, B.A., Prospero, J.M., Mackie, D., Gaiero, D., Hesse, P.P., Balkanski, Y., 2010. Global connections between aeolian dust, climate and ocean biogeochemistry at the present day and at the last glacial maximum. Earth Sci. Rev. 99 (1–2), 61–97.
Marsham, J.H., Parker, D.J., Grams, C.M., Johnson, B.T., Grey, W.M.F., Ross, A.N., 2008. Observations of mesoscale and boundary-layer scale circulations affecting dust transport and uplift over the Sahara. Atmos. Chem. Phys. 8, 6979–6993.
Martin, J.H., 1990. Glacial-interglacial CO_2 change: the iron hypothesis. Paleoceanography 5, 1–13.
McGinnigle, 1966. Dust whirls in north-west Libya. Weather 21, 272–276.
Miller, R., Tegen, I., Perlwitz, J., 2004. Surface radiative forcing by soil dust aerosols and the hydrologic cycle. J. Geophys. Res.: Atmospheres 109 (D4), JD004085.
Mlawer, E.J., Taubman, S.J., Brown, P.D., Iacono, M.J., Clough, S.A., 1997. RRTM, a validated correlated-k model for the longwave. J. Geophys. Res. 102, 16663–16682.
Natsagdorja, L., Jugdera, D., Chung, Y.S., 2003. Analysis of dust storms observed in Mongolia during 1937-1999. Atmos. Environ. 37 (9/10), 1401–1411.
Obukhov, A.M., 1971. Turbulence in an atmosphere with a non-uniform temperature. Boundary-Layer Meteorol. 2 (1), 7–29.
Oke, A.M.C., Tapper, N.J., Dunkerley, D., 2007. Willy willies in the Australian landscape: the role of key meteorological variables and surface conditions in defining frequency and spatial characteristics. J. Arid Environ. 71, 201–215.
Overpeck, J., Rind, D., Lacis, A., Healy, R., 1996. Possible role of dust-induced regional warming in abrupt climate change during the last glacial period. Nature 384, 447–449.
Petit, J.R., Jouzel, J., Raynaud, D., Barkov, N.I., Barnola, J.M., Basile, I., Bender, M., Chappellaz, J., Davis, M., Delaygue, G., Delmotte, M., Kotlyakov, V.M., Legrand, M., Lipenkov, V.Y., Lorius, C., Pepin, L., Ritz, C., Saltzman, E., Stievenard, M., 1999. Climate and atmospheric history of the past 420,000 years from the Vostok ice core, Antarctica. Nature 399, 429–436.
Rafkin, S., Jemmett-Smith, B., Fenton, L., Fenton, L., Lorenz, R., Takemi, T., Ito, J., Tyler, D., 2016. Dust devil formation. Space Sci. Rev. 203 (1–4), 183–207.
Renno, N.O., Burkett, M.L., Larkin, M.P., 1998. A simple thermodynamical theory for dust devils. J. Atmos. Sci. 55, 3244–3252.
Ridgwell, A.J., 2002. Dust in the Earth system: the biogeochemical linking of land, air and sea. Philos. Trans. A Math. Phys. Eng. Sci. Dec. 15, 2905–2924 360(1801).
Ryan, J.A., 1972. Relation of dust devil frequency and diameter to atmospheric temperature. J. Geophys. Res. 77 (36), 7133–7137.
Shao, Y., 2001. A model for mineral dust emission. J. Geophys. Res. 106 (D17), 20239–20254.
Shapiro, A., Kogan, Y.L., 1994. On vortex formation in multicell convective clouds in a shear-free environment. Atmos. Res. 33 (1–4), 125–136.
Sinclair, P.C., 1964. Some preliminary dust devil measurements. Mon. Weather Rev. 22 (8), 363–367.
Sinclair, P.C., 1969. General characteristics of dust devils. J. Appl. Sci. 30, 1599–1619.
Sinclair, P.C., 1973. The lower structure of dust devils. J. Atmos. Sci. 30, 1599–1619.
Skamarock, W.C., Klemp, J.B., Dudhia, J., Gill, D.O., Barker, D.M., Duda, M.G., Huang, X., Wang, W., Powers, J.G., 2008. A Description of the Advanced Research WRF version 3. NCAR Tech. Note, NCAR/TN-475 + STR, 8 pp. Natl. Cent. for Atmos. Res., Boulder, CO, USA Available at: http://www.mmm.ucar.edu/wrf/users/docs/arwv3.pdf.
Snow, J.T., McClelland, T.M., 1990. Dust devils at White Sands Missile Range, New Mexico: 1. Temporal and spatial distributions. J. Geophys. Res. 95 (D9), 13707–13721.
Sokolik, I.N., Winker, D.M., Bergametti, G., Gillette, D., Caarmichael, G., Kaufman, Y., Gomes, L., Schuetz, L., Penner, J., 2001. Introduction to special section: outstanding problems in quantifying the radiative impacts of mineral dust. J. Geophys. Res. 106, 18015–18027.
Sun, J.M., Ding, Z.L., Liu, T.S., 1998. Desert distributions during the glacial maximum and climatic optimum: example of China. Episodes 21, 28–31.
Tanaka, T.Y., Chiba, M., 2006. A numerical study of the contributions of dust source regions to the global dust budget. Global Planet. Change 52 (1), 88–104.
Toigo, A.D., 2003. Numerical simulation of Martian dust devils. J. Geoghys. Res. 108 (E6) 1–1-1-14.
Tratt, D.M., Hecht, M.H., Catling, D.C., Samulon, E.C., Smith, P.H., 2003. In situ measurement of dust devil dynamics: toward a strategy for Mars. J. Geophys. Res.: Planets (1991-2012) 108 (E11), 5116.
Twomey, S., Piepgrass, M., Wolfe, T.L., 1984. An assessment of the impact of pollution on global cloud albedo. Tellus B 36, 356–366.
Wang, C., Wei, Z.G., Li, Z.C., Liu, H., Wei, H., 2011. The variation characteristics of difference between surface and air temperature in Dunhuang Gobi. J. Arid Land Resour. Environ. 25 (11), 72–78.
Werner, M., Tegen, I., Harrison, S., Kohfeld, K.E., Prentice, I.C., Balkanski, Y., Rodhe, H., Roelandt, C., 2002. Seasonal and interannual variability of the mineral dust cycle under present and glacial climate conditions. J. Geophys. Res.: Atmos. 107 (D24) AAC2-1-AAC 2–19.
Wu, C.L., Lin, Z.H., 2014. Impact of two different dust emission schemes on the simulation of a severe dust storm in East Asia using the WRF/Chem model. Clim. Environ. Res. (in Chinese) 19 (4), 419–436.
Zhao, T.L., Gong, S.L., Zhang, X.Y., Jaffe, D.A., 2008. Asian dust storm influence on North American ambient PM levels: observational evidence and controlling factors. Atmos. Chem. Phys. 8, 2717–2728.